



ACADEMIC
PRESS

Available online at www.sciencedirect.com

SCIENCE @ DIRECT®

Journal of Structural Biology 143 (2003) 124–134

Journal of
Structural
Biology

www.elsevier.com/locate/yjsbi

The 10.8-Å structure of *Saccharomyces cerevisiae* phosphofructokinase determined by cryoelectron microscopy: localization of the putative fructose 6-phosphate binding sites

Teresa Ruiz,^{a,*} Ingrid Mechin,^b Jörg Bär,^c Wojciech Rypniewski,^{d,e}
Gerhard Kopperschläger,^c and Michael Radermacher^a

^a Department of Molecular Physiology and Biophysics, University of Vermont College of Medicine, Burlington, VT 05405, USA

^b EMBL Hamburg Outstation, EMBL c/o DESY, Notkestrasse 85, D-22603 Hamburg, Germany

^c Institut für Biochemie, Medizinische Fakultät, Universität Leipzig, Liebigstrasse 16, D-04103 Leipzig, Germany

^d Institute of Bioorganic Chemistry, Polish Academy of Sciences, Noskowskiego 12/14, 61-704 Poznan, Poland

^e Institute of Medical Biochemistry and Molecular Biology, University Hospital Hamburg c/o DESY, Building 22a, Notkestrasse 85, 22603 Hamburg, Germany

Received 21 May 2003, and in revised form 10 July 2003

Abstract

Phosphofructokinase plays a key role in the regulation of the glycolytic pathway and is responsible for the phosphorylation of fructose 6-phosphate to fructose 1,6-bisphosphate. Although the structure of the bacterial enzyme is well understood, the knowledge is still quite limited for higher organisms given the larger size and complexity of the eukaryotic enzymes. We have studied phosphofructokinase from *Saccharomyces cerevisiae* in the presence of fructose 6-phosphate by cryoelectron microscopy and image analysis of single particles and obtained the structure at 10.8 Å resolution. This was achieved by optimizing the illumination conditions to obtain routinely 8-Å data from hydrated samples in an electron microscope equipped with an LaB₆ and by improving the image alignment techniques. The analysis of the structure has evidenced that the homology of the subunits at the sequence level has transcended to the structural level. By fitting the X-ray structure of the bacterial tetramer into each dimer of the yeast octamer the putative binding sites for fructose 6-phosphate were revealed. The data presented here in combination with molecular replacement techniques have served to provide the initial phases to solve the X-ray structure of the yeast phosphofructokinase.

© 2003 Elsevier Inc. All rights reserved.

Keywords: Phosphofructokinase; *Saccharomyces cerevisiae*; Glycolytic enzyme; Vitreous ice; Three-dimensional reconstruction; Electron microscopy; Simultaneous alignment; Radon transforms; CTF correction; Point mode; X-ray

1. Introduction

Adenosine triphosphate (ATP) is a universal source of free energy in living cells. Organisms opt to produce ATP either through a higher rate but lower yield pathway (glycolysis) or through a lower rate but higher yield pathway (respiration) depending on the available energy resources. Most unicellular organisms use glycolysis as

their main pathway for energy production. The phosphorylation of fructose 6-phosphate (Fru 6-P) by phosphofructokinase (Pfk-1; EC 2.7.1.11) in the presence of magnesium and ATP is the first irreversible step specific for the glycolytic pathway. The key role that Pfk-1 plays in the regulation of glycolysis is evidenced by the large number of allosteric effectors that control its enzymatic activity (Heinrich et al., 1977; Hofmann, 1976; Kotlarz and Buc, 1982; Uyeda, 1979).

Understanding the mechanisms of catalysis and regulation of Pfk-1 from different sources has been the focus of a great number of studies in the past years. The

* Corresponding author. Fax: 1-802-656-0747.

E-mail address: truiz@physiology.med.uvm.edu (T. Ruiz).

largest success has been achieved for the less complex bacterial enzyme (e.g., *Escherichia coli*, *Bacillus stearothermophilus*). Bacterial phosphofructokinases are homotetramers with a total molecular weight of 140 kDa (Blangy, 1968) and their activity is mainly regulated by only two effectors, an activator (adenosine diphosphate; ADP) and an inhibitor (phosphoenol pyruvate; PEP) (Evans, 1992). The bacterial subunits are elongated and are composed of two domains, a small domain that binds Fru 6-P and a large domain that binds ATP. Each of these domains has the characteristic structural pattern found in glycolytic enzymes with a core of parallel β strands surrounded by α helices. Of the three binding sites available per subunit, two of them form the active site binding Fru 6-P and ATP, while the third, the allosteric site, binds either PEP or ADP. Essentially, the tetramers can be considered as dimers of dimers presenting small interactions between dimers, where the Fru 6-P binding site is located, and large interactions between the subunits in each dimer, where the effectors bind. Crystallographic structures available at different stages in the reaction (in the presence of substrates, products, and/or effectors) have elucidated the conformational changes that occur and led to an understanding of the mechanism of substrate binding and catalysis for the bacterial enzyme (Evans and Hudson, 1979; Evans et al., 1986; Rypniewski and Evans, 1989; Shirakihara and Evans, 1988). Briefly, a conformational change takes place from the open to the closed state bringing the two substrates together through a 7° rotation of one dimer relative to the other.

The information about the bacterial enzyme represents a great advancement in the understanding of this step in the glycolytic pathway; however, our knowledge of the enzyme is still limited for higher organisms. Eukaryotic phosphofructokinases are more complex structures and, due to the larger number of effectors that act upon them, exhibit a far more complicated regulatory mechanism (Sols, 1981). An excellent example is fructose 2,6-bisphosphate (Fru 2,6-P₂), a product of the gluconeogenesis pathway, which is a potent activator of Pfk-1 only in eukaryotes and serves as a linker between glycolysis and gluconeogenesis (van Schaftingen, 1987).

The “double-size” subunits of the eukaryotic enzymes have arisen through a process of gene duplication and fusion of the bacterial gene (Heinisch, 1986; Poorman et al., 1984). In this process, the catalytic Fru 6-P binding site in the second bacterial gene product (the C-terminal half of the eukaryotic subunit) has been transformed into an effector binding site and acquired a regulatory role, thus providing more flexibility for regulation. Mammalian enzymes are tetrameric structures composed of three different subunits (m, muscle; l, liver; and p, platelet) in various stoichiometries that are tissue dependent. Yeast phosphofructokinases are either homooctameric (*Schizosaccharomyces pombe*) (Reuter

et al., 2000) or heterooctameric structures (*Saccharomyces cerevisiae*, *Kluyveromyces lactis*, *Candida albicans*) (Bär et al., 1997; Kopperschläger et al., 1977; Lorberg et al., 1999; Plietz et al., 1978; Reuter et al., 2000; Tijane et al., 1979), the α and β subunits having evolved by a second gene duplication event. The analysis of amino acid sequences shows that there is a 55% identity between the α and the β subunits in yeast and a 41% identity of either yeast subunit with the mammalian subunits. However, no significant homology was observed between the first 200 amino acids in the N-terminal domain of the subunits.

Despite the great pool of biochemical and molecular knowledge available for eukaryotic phosphofructokinases, their structures are still unknown mostly due to the lack of good quality crystals. The best characterized of the eukaryotic enzymes is the Pfk-1 from *S. cerevisiae*. This enzyme contains two types of subunits, an α subunit of 987 residues and a β subunit of 959 residues (Heinisch et al., 1989). The native enzyme, with a sedimentation coefficient of 21S, is a heterooctamer of 835 kDa, composed of four α and four β subunits (Kopperschläger et al., 1977). The yeast Pfk-1 exhibits cooperative binding for Fru 6-P and noncooperative binding for ATP (Reuter et al., 1979). In addition, as for most eukaryotic organisms and in contrast to the bacterial enzyme, yeast Pfk-1 is allosterically activated by Fru 2,6-P₂ and adenosine monophosphate (AMP) (Nissler et al., 1983) and inhibited by ATP (Larsson et al., 2000; Laurent et al., 1978; Nissler et al., 1977b). The current hypothesis, based on biochemical experiments that show the cooperativity of Fru 2,6-P₂ and AMP in the activation of Pfk-1 (Nissler et al., 1984), proposes the existence of two distinct binding sites, one for the sugar and another for the nucleotide effectors.

The octameric structure of the *S. cerevisiae* Pfk-1 was first confirmed by small-angle X-ray scattering experiments (Plietz et al., 1978) and later by a negative stain interconversion study of two-dimensional averages (Nissler et al., 1985). Eventually, the first low-resolution (20 Å) three-dimensional structure of the enzyme in the presence of Fru 6-P was obtained by cryoelectron microscopy (Ruiz et al., 2001). This study revealed the shape of the subunits and their mutual arrangement in the octamer and also an unexpected asymmetry between the two $\alpha_2\beta_2$ tetramers of the molecule. The calculated radius of gyration of the structure was consistent with the reported values from small-angle X-ray scattering experiments (Laurent et al., 1978; Plietz et al., 1978).

We have continued our analysis of Pfk-1 from *S. cerevisiae* by cryoelectron microscopy and here we report the structure at 10.8 Å resolution. The results of fitting the *E. coli* tetramer into the three-dimensional volume have allowed us to elucidate the position of the Fru 6-P binding sites in the yeast structure.

2. Materials and methods

2.1. Enzyme purification

Pfk-1 was purified from a recombinant strain of *S. cerevisiae* carrying a multicopy vector of the PFK1 and PFK2 genes, kindly supplied by Dr. J. Heinisch (Düsseldorf, Germany), according to Hofmann and Kopperschläger (1982) with minor modifications. Chemicals were at least of analytical grade and unless otherwise specified, all the purification steps were carried out at 4°C.

Approximately 150 g of yeast suspended in 300 ml of buffer A (50 mM sodium phosphate buffer, pH 7.2, containing 5 mM 2-mercaptoethanol and 0.5 mM phenylmethylsulfonyl fluoride) were disrupted in a Vibrogen Cell Mill (Bühler, Germany) for 5 min with continuous cooling of the jacket vessel at 4°C. The cell debris was pelleted by centrifugation at 17000g for 30 min and discarded. The supernatant was then subjected to two fractionated precipitations with PEG 6000 at 4 and 12%, respectively. The first pellet was discarded. After a final centrifugation at 17000g for 30 min, the pellet was resuspended in 300 ml of buffer A. Affinity-gel chromatography on Cibacron blue F3G-A-Sephadex G-100 was performed in a batch mode. After the affinity gel was washed thoroughly with buffer A to remove unbound protein, the enzyme was desorbed with buffer A complemented with 5 mM ATP and 10 mM MgCl₂. After precipitation of the enzyme in the eluate with ammonium sulfate at 80% saturation, the pellet was dissolved in buffer A and subjected to gel filtration on a Sepharose 6B gel-filtration column previously equilibrated with buffer A and ammonium sulfate at 30% saturation. All the fractions that showed enzyme activity were pooled together and subjected to a new ammonium sulfate precipitation at 80% saturation. The pellet was dissolved in a minimal volume of buffer A, desalted on a PD10 column (Amersham Pharmacia), and then applied to a Resource Q anion-exchange column equilibrated with buffer A. After the column was washed until the eluate was free of protein, the enzyme was eluted by applying a linear gradient of KCl (0–300 mM) in buffer A. Finally, all fractions showing Pfk-1 activity were pooled together, precipitated with ammonium sulfate at 80% saturation, and stored at 4°C and a final concentration of 10 mg/ml in buffer A saturated with ammonium sulfate.

2.2. Electron microscopy

A small aliquot (10–20 µl) of the enzyme suspension was run through a Micro Bio Spin P-30 column (Bio-Rad), previously equilibrated with 50 mM sodium phosphate buffer containing 3 mM Fru 6-P (pH 7.2), to remove the ammonium sulfate. The protein was diluted

to 40–10 µg/ml and applied to 400-mesh copper holey grids coated with a thin carbon film. The grids were blotted at 4°C using a double-blotting device and rapidly frozen in liquid ethane cooled at liquid nitrogen temperatures. Samples were observed using a cryoholder (Gatan) on a CM120 Philips electron microscope (FEI, Holland) equipped with an anticontaminator (Gatan) and an LaB₆ cathode (Kimball, USA) operated in *point mode*.¹

The illumination conditions were optimized at three points in the optical path to obtain the highest coherence: (a) gun, (b) condenser 1 (C₁), and (c) condenser 2 (C₂).

- The LaB₆ filament was mounted in a Wehnelt cylinder with a 0.3-mm aperture and the distance between the tip and the aperture (filament height) was set to 0.12–0.13 mm. Filaments were always operated below saturation in a mode referred to as *point mode*.
- The best combination of C₁ excitation (“spot size”) and C₂ aperture was established by observing the power spectrum of images recorded with a CCD camera under varying illumination conditions. The best coherence conditions (largest extent of Thon rings) were found to be achieved with a C₂ aperture of 100 µm and a spot size of 4, for the available apertures with diameters of 200, 100, and 50 µm.
- The beam (C₂) was overfocused to cover at least the area of the large viewing screen.

These settings have allowed us to routinely obtain images from frozen hydrated samples with visible Thon rings out to a resolution of better than 10 Å (typically 8 Å).

Negatives were recorded under low-dose conditions on S0-163 Kodak film at an accelerating voltage of 100 kV and a nominal magnification of 60000×. The 0° tilt images were collected at defoci ranging from 1 to 3.5 µm to ensure a good coverage of Fourier space. The electron dose used for each image was approximately 1000 e⁻/nm².

2.3. Image analysis

Negatives with diffractograms showing Thon rings beyond 11 Å were selected and digitized with a 7-µm raster size on a SCAI flat-bed scanner (Zeiss, Germany). Images were binned three times to obtain a final pixel size of 0.36 nm on the sample scale (calibrated magnification of 58300×). Sixteen thousand particles were selected, windowed into images with dimensions corresponding to approximately twice the particle diameter, and normalized with the image average. Image

¹ We would like to give credit for this usage, but we have not been able to find any reference to this mode in the literature.

processing was carried out using the program SPIDER (version 5.0, with modifications).

The image processing strategy can be divided into three steps: an initial rough alignment of the projections to an existing volume, an intermediate low-resolution alignment, and a final high-resolution alignment. First the projections were translationally and rotationally aligned to a volume with 2-nm resolution calculated from 6000 images acquired under the same conditions (Ruiz et al., 2001). The search was carried out over the entire Fourier space using Radon alignment algorithms (Radermacher, 1997, 2001) in 30° angular increments and a strongly low-pass-filtered reference (7 nm) to minimize the bias of the alignment by the reference. The aligned projections were used to create a new volume that, properly filtered to low resolution, was used as reference for the following alignment. Several rounds (~10) of translational/rotational alignment were carried out and the search range was confined more and more after each of them. After each alignment a new volume was calculated to be used as reference for the next alignment. The resolution of the volume was determined by Fourier shell correlation (Saxton and Baumeister, 1982; Stewart et al., 1999; van Heel et al., 1982) using a cut-off criterion of five times the noise correlation (FSC₅). The reference volume was low-pass filtered to a resolution 115% of the calculated resolution (e.g., resolution 2.0 nm; filter 2.3 nm). To obtain a good coverage of the Fourier space, images were collected at different defoci. The transfer function correction was performed as described in Radermacher et al. (2001). Periodograms were calculated for each micrograph (Fernandez et al., 1997) and the defocus and astigmatism were determined. The images were corrected by flipping the sign of the Fourier components accordingly, using a smooth function. No other corrections were applied (e.g., no temperature factor was applied to boost the high frequencies). A new reconstruction was calculated from the corrected images and used as the starting reference for another set of refinement steps. Several more rounds of translational/rotational alignments were carried out until the orientation of the projections was stable to 0 pixels of translational shift and $\pm 2^\circ$ of angular shift, then a volume was calculated and its resolution determined.

After having a stable volume at low resolution we started a new set of refinement steps (see Section 4). During these refinements the reference volumes were not only low-pass filtered to 115% of their measured resolution (e.g., resolution 2.0 nm; filter 2.3 nm) but were also high-pass filtered to 1/2 of the particle diameter. The overall alignment was done as before with the search parameters for the whole process given by translational shift of 1 pixel and angular shifts of $\pm 6^\circ$ in angular increments of 1°. The refinement process was finished when the orientation of the projections was

stable to 0 pixels of translational shift and $\pm 1^\circ$ of angular shift. At this point, a final volume was calculated and its resolution determined as before.

The high-resolution volume was converted from Spider format to brix format and the *E. coli* tetramer (PDB i.d: 2pfk) (Rypniewski and Evans, 1989) was fitted manually in the framework of the program “O” (Jones et al., 1990).

3. Results

A three-dimensional reconstruction of phosphofruktokinase from *S. cerevisiae* was calculated from 16000 images extracted from negatives collected at different defoci from vitreous ice preparations (Fig. 1A). The periodograms (in which the 2.3- and 1.15-nm layer lines of tobacco mosaic virus are visible) show the quality of the data (Fig. 1B). To achieve full coverage in Fourier space 75 negatives with defoci ranging between 1.0 and 3.5 μm were used. An average periodogram calculated from all the periodograms showed that all the frequencies were well represented (not shown).

In a previous study we had proven that the particles fell on the carbon in different orientations with virtually no variability in shape (Ruiz et al., 2001). Therefore in

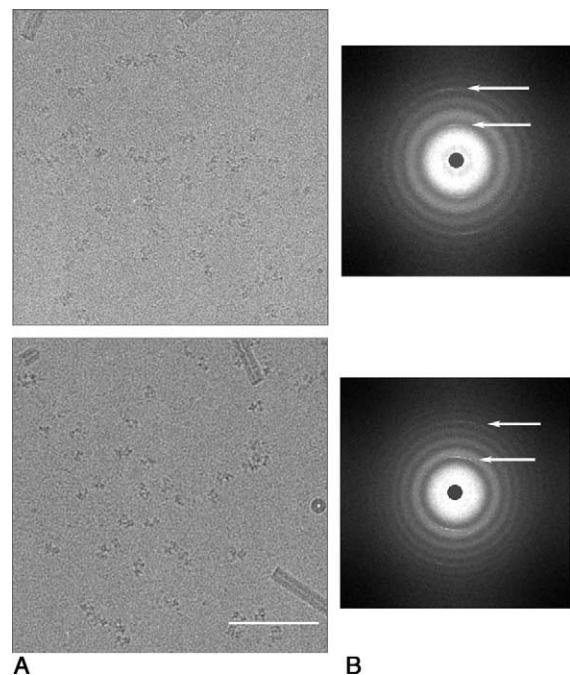


Fig. 1. (A) Areas from two micrographs of phosphofruktokinase from a vitreous ice preparation used for the three-dimensional reconstruction. The rod-like particles are tobacco mosaic virus (TMV), which were used for magnification calibration. (B) Average periodograms calculated from the complete micrographs showing the transfer of data to 8–9 Å. The arrows point to the 2.3- and 1.15-Å layer lines of TMV. The defoci of the images are approximately 1.1 and 2.2 μm . Scale bar, 100 nm.

this particular case we have been able to calculate a reconstruction using reference-based three-dimensional projection alignment methods and only 0° tilt images. An additional radial slice (P slice) has been implemented in the three-dimensional Radon transform to act as a counter which shows the occupancy of each radial line in the transform and can be used to follow the angular coverage of the projection space. Thus, during the alignment procedure the angular coverage was surveyed after each step by displaying the last P slice of the three-dimensional Radon transform created after each alignment. The new calculated volume was used as a new reference in the following alignment step. At the beginning of the alignment the coverage follows the angular search increment (e.g., coverage in 12° intervals after searching with 12° angular increments). Using angular increments that are not multiples of each other it is possible to cover evenly the entire angular space. Once the angles for the orientations of the projections are known it is easy to calculate a plot that shows the final angular distribution of the particle orientations (Fig. 2). The plot shows that all projecting directions are well covered. In particular, the good coverage at the periphery of the disk shows that most of the projections represent a fully occupied single-axis tilt series around the long axis of the particle. The complete coverage was corroborated by the data in the last P slice of the three-dimensional Radon transform which showed that every radial line was filled by contributions from more than one projection.

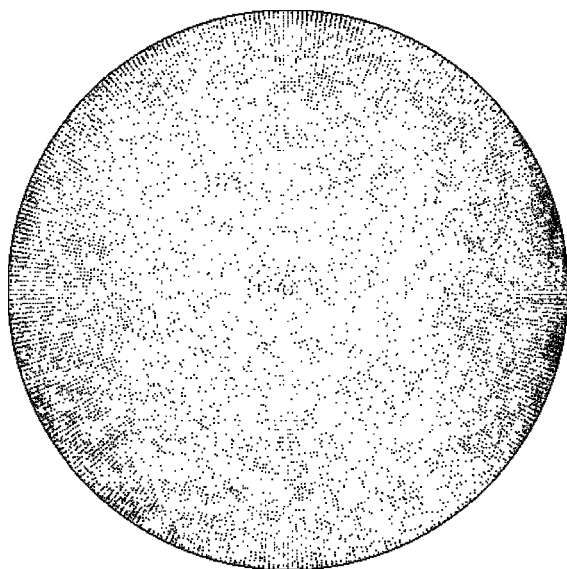


Fig. 2. The angular coverage of the projection space is depicted. The azimuthal coordinate corresponds to the rotation of the molecule around its long axis, the radial coordinate to the cosine of the tilt angle around a space-fixed-axis parallel to the short axis of the molecule. The plot shows that all projecting directions were well covered. Especially the good coverage at the periphery of the circle shows that the majority of the projections combine to a fully occupied single-axis tilt series.

Resolution curves were calculated at different steps of alignment procedure (see Section 2). In Fig. 3 we can see how the resolution changed between the low-resolution volume after CTF correction and refinement ($FSC_5 = 15.2 \text{ \AA}$), the volume after three rounds of alignment using a high-pass filter ($FSC_5 = 12.6 \text{ \AA}$), and the final reconstruction after five additional rounds of refinement, in which approximately 5% of the particles showing low cross-correlation values were excluded ($FSC_5 = 10.8 \text{ \AA}$). It should be noted that using this method not only the high frequencies were improved but also the overall quality of the alignment. This improvement in resolution was attained with minimal changes in the orientations of the projections. After eight rounds of refinement using combined low- and high-pass filters, the median angular change between the initial and the final orientations of the 16 000 projections was only 4° (the mean was 4.5°).

The finer detail inherent in the new reconstruction is evident if we compare *X* and *Z* sections of the volume with those we published earlier (Fig. 4). In general, the new sections reveal enhanced contrast, better defined densities, and lower noise. In addition, ghost densities external to the molecule have mostly disappeared. A careful comparison of the second *X* section (**) reveals now much clearer connections between the dimers of the bottom tetramer. This is even more apparent when looking at the corresponding *Z* sections (***) in which the broad central connections have narrowed into thin lines. The surface representations shown in Fig. 5 confirm all the above observations. The surface, which was smooth in the old reconstruction, shows a substantially more detailed texture. In the top left view the interactions between the upper (U) and the lower (L) domains of the top tetramer have become stronger and a twofold axis perpendicular to this face of the molecule is now clearly visible. The striking difference between the top

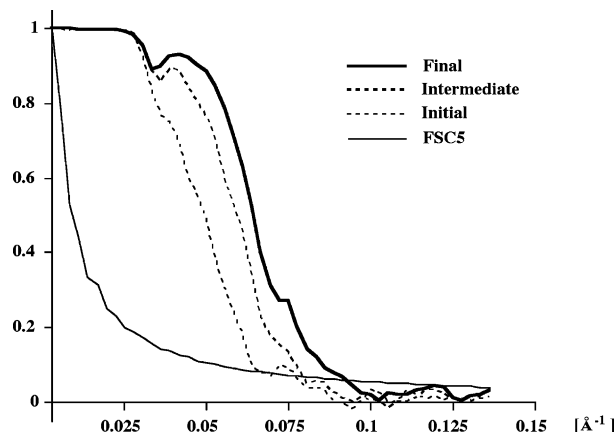


Fig. 3. Resolution curves at different stages of the alignment process. The final resolution was 10.8 \AA using the five times noise correlation criteria (see text for details).

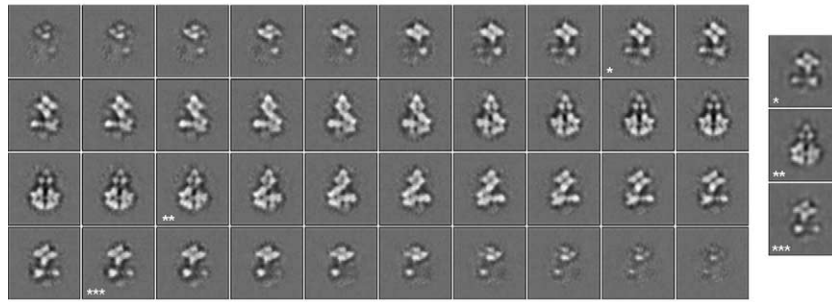
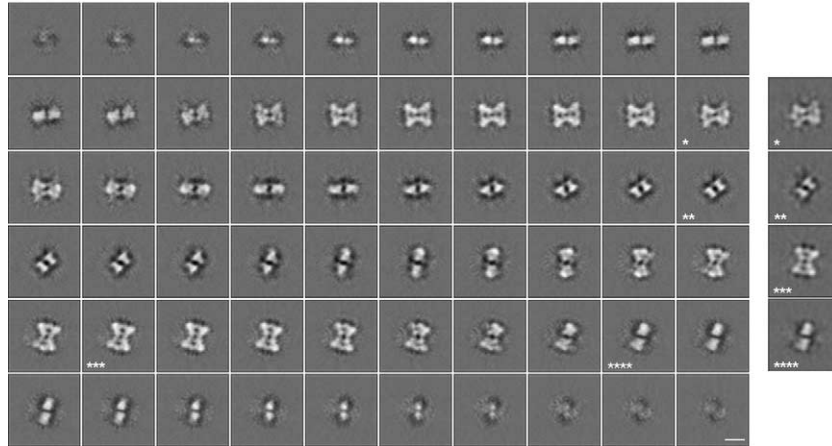
A X-sections**B Z-sections**

Fig. 4. (A) *X* slices through the three-dimensional reconstruction. (B) *Z* slices through the reconstruction. To the right the slices from our previous low-resolution reconstruction (20 Å) are shown. The corresponding slices of the two reconstructions are marked with asterisks. The higher resolution becomes most obvious when observing the thin connections between either dimers or tetramers, visible in the central *X* slices.

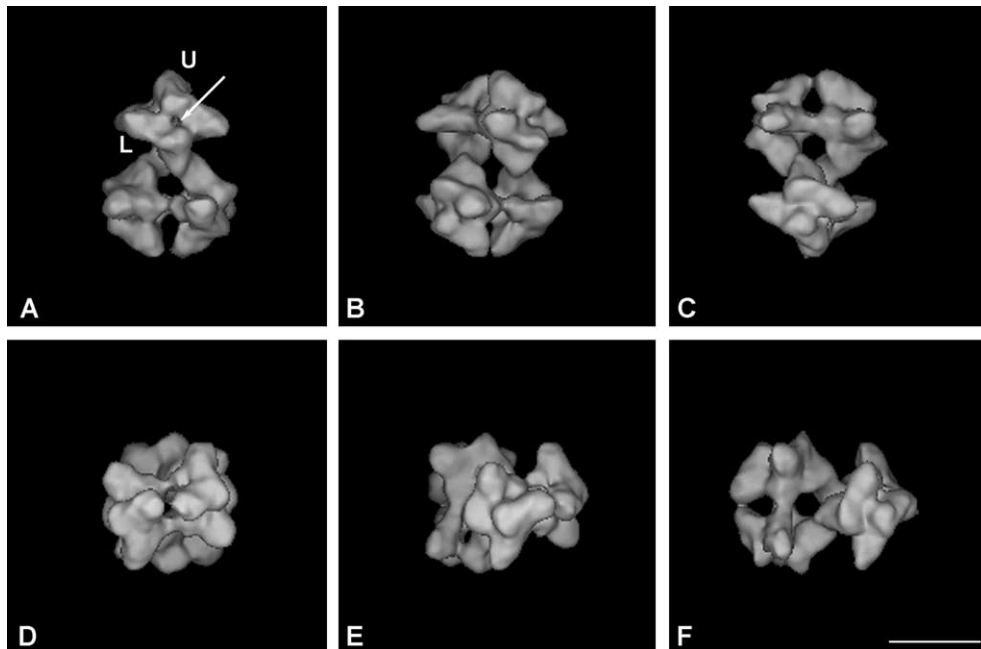


Fig. 5. Surface views of the reconstruction thresholded using the criterion of maximum steepness of the density of contour lines. (A, B, C) Views perpendicular to the long axis of the molecule rotated by 90° relative to each other. (D, E, F) Views perpendicular to the short axis of the molecule rotated by 90° relative to each other. U is the upper domain and L the lower domain of the tetramer. The arrow points to the twofold axis of the tetramer. Scale bar, 10 nm. Views A and D can be compared with those shown in Fig. 6.

and the bottom tetramers that we observed previously is also present in our high resolution reconstruction (see Figs. 5A and C). The two domains (L and U) appear sheared with respect to each other, moving closer to each other in the bottom tetramer, thus closing the gap between them. In the bottom left view (Fig. 5D) we can now observe a channel-like opening that leads from the bottom of the molecule all the way to the top. Overall this volume encompasses approximately 137% of the molecular weight as expected for limited-resolution reconstructions (e.g., Frank and Agrawal, 1998; Mouche et al., 1999). Moreover, the calculated radius of gyration for the molecule ($R_G = 7.0$ nm) is in excellent agreement with both the value obtained with our prior reconstruction and those reported from small-angle X-ray scattering experiments (7.4 ± 0.2 nm, Plietz et al., 1978; and 7.0 ± 0.1 nm, Laurent et al., 1978).

At this high resolution the surfaces of both the top tetramer (Fig. 5A) and the bottom tetramer (Fig. 5C) highly resemble the surface view along the r axis of the *E. coli* phosphofructokinase. We have fitted manually *E. coli* tetramers into all four possible positions of the yeast octamer using the program “O”; only the fit of two of these tetramers is shown in Fig. 6 for better visualization. These positions are unique, displacements of only one pixel (3.6 Å) resulted already in clearly visible mismatches. It should be noted that one *E. coli* tetramer represents only two-thirds of the molecular weight of a yeast dimer. The empty spaces in the yeast volume will be filled with the extra mass (70 kDa) present at the C and N termini of the yeast subunits. The void areas are mainly located at the distal ends and at the center of the yeast Pfk-1. The latter is in agreement with the fact that

E. coli tetramers do not readily form higher aggregates and therefore some of the additional amino acids from the yeast subunits should be at the center forming the interaction between the two tetramers. Taking a closer look at just one of the fitted *E. coli* tetramers we can identify the four possible Fru 6-P binding sites (Fig. 7, right). Two of these sites are located on the inner surface of the yeast dimer, facing the channel-like opening, and the other two are on the external surface of the yeast dimer. In this external surface the Fru 6-P binding sites are positioned very close to the connection between the upper and the lower domains that we have described previously (U and L in Fig. 5A), specifically in a region where the protein density is relatively low.

4. Discussion

We present here the three-dimensional reconstruction of phosphofructokinase from *S. cerevisiae* at 10.8 Å resolution calculated in the presence of Fru 6-P from 16 000 projections extracted from 0° tilt images of the specimen in vitreous ice.

There are three critical elements that have contributed to obtaining such a high-resolution structure from a comparatively small number of images. Two of them are technical (improvement of both the image acquisition and the image processing techniques) and the third is inherent in the molecule itself. In essence we have first enhanced the overall quality of the images by improving the coherence of the electron beam using an electron microscope just equipped with just an LaB₆ filament running in point mode (for more details, see Section 2).

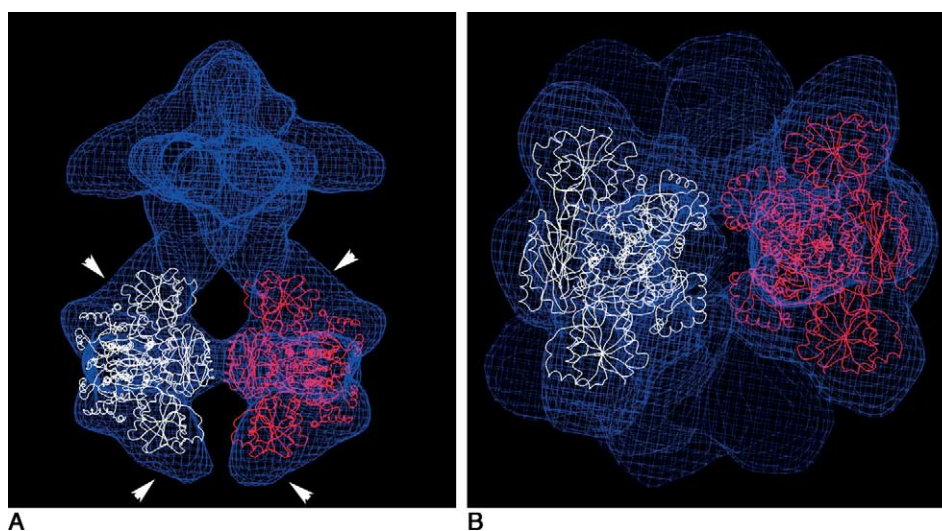


Fig. 6. Four *E. coli* Pfk-1 tetramers fit into the whole yeast Pfk-1. Two *E. coli* Pfk-1 tetramers fit into one of the yeast Pfk-1 tetramers. For better visibility only the fit into the bottom tetramer is shown. The fit of the two additional *E. coli* Pfk-1 tetramers into the top yeast tetramer would be analogous. The arrowheads point to the empty spaces in the yeast volume which should be filled with the additional mass of the yeast subunits. (A) View perpendicular to the long axis of the molecule. (B) View perpendicular to the short axis of the molecule. Each *E. coli* tetramer is shown in a different color.

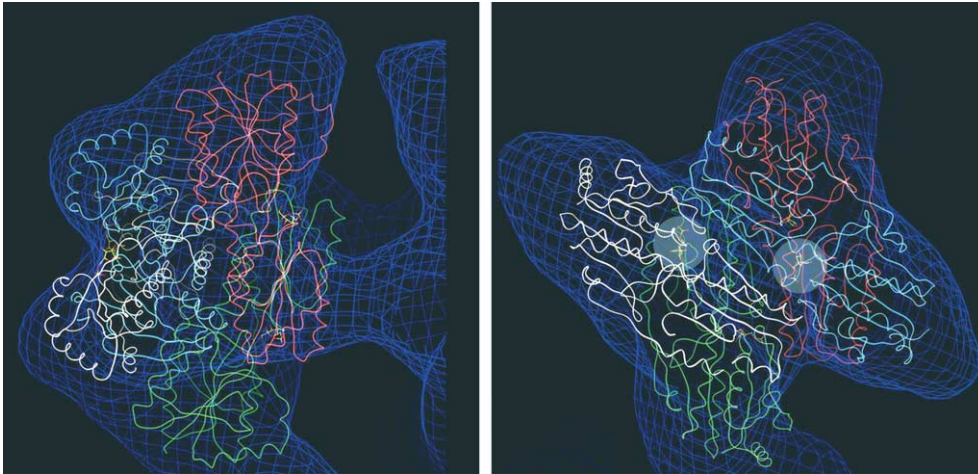


Fig. 7. Fit of one *E. coli* Pfk-1 tetramer into a yeast dimer. Each subunit of the *E. coli* tetramer is shown in a different color. The four possible Fru 6-P binding sites per yeast dimer are shown (Fru 6-P is shown as a stick model in red and yellow). The white disks highlight the two putative catalytic sites.

The images that we routinely obtain are more characteristic of electron microscopes equipped with field emission guns. All the images used in our study showed significant information well beyond 11.5 Å (Fig. 1) even at the large defoci (1–3.5 μm) necessary to visualize single particles and achieve a good coverage of all the spatial frequencies in Fourier space. The subdivision of the whole processing scheme into two major steps, an initial step in which mainly the low-resolution features are aligned and a second step in which more weight is given to the high-resolution details, has also proved decisive for achieving our goal. Using only a low-pass filter or a combination of low-pass filter and mild high-pass filter, to account for the unevenness of the background on the image, might be biasing the alignment toward the low-resolution information. Images taken with smaller defoci will have weaker signal at low resolution than those with higher defoci and will show smaller cross-correlation values. This bias can be avoided by applying a specimen-adapted band-pass filter. By running a few additional rounds of refinement using only the information in the resolution range between 1/2 particle diameter and 115% of the reference volume resolution, and searching for the optimal orientation of the projections in the close neighborhood of the prior orientation, we have been able to attain a dramatic improvement in the resolution of the three-dimensional structure with just minor rearrangements of the projections (Fig. 3).

Several characteristics of the sample have further aided the achievement of high resolution. Its homogeneity was proven earlier by the comparison of three-dimensional reconstructions from random conical data sets (Ruiz et al., 2001). In this previous study only two forms of the molecule were found, a small number of half-molecules (tetramers) and a majority of intact octameric

structures. These large size differences were the only difference found and it is easy to differentiate between these two forms even in 0° micrographs without any additional tilting. Thus, we were able to attribute all other differences observed in the sample to differences in particle orientation. Zero-degree images of frozen hydrated specimens are easier to collect and charging effects are much less of a problem when no tilt is required. The resolution that can be achieved in 0° images is normally better than the resolution of images of a highly tilted specimen. Additionally the molecule was found preferably lying with its long axis positioned parallel to the carbon support film. The shape of the molecule favors this orientation and the angular differences are predominantly rotations around its long axis. These rotations were quite evenly distributed and the data set represents essentially a single axis tilt series with a full 360° rotation. All these factors, the absence of a requirement for collecting tilt data, the high resolution of the 0° images, and the full angular coverage, have contributed to the high resolution in three dimensions that we have been able to achieve.

This reconstruction has opened the path toward understanding not only the complicated structure of the yeast Pfk-1 but also its function. If we subdivide the yeast octameric enzyme into smaller building blocks, like tetramers and dimers, it is possible to establish an equivalence between the yeast dimer and the “bacterial tetramer.” However, it should be kept in mind that under these conditions, one-third of the molecule is unaccounted for. During the process of gene duplication and fusion a long amino acid sequence (200 residues) was added to the N-terminal domain and ~80 residues to the C-terminal domain.

The uniqueness of the fit of the *E. coli* tetramers into the yeast dimers shows that nature has not only used the

ancestral bacterial gene as the genetic building block but has also used the bacterial tetramer as the structural building block for eukaryotic enzymes. As we pointed out under Section 3, most of the void areas are located in the central region of the octameric structure serving as links between the two tetramers. The additional amino acids of the C- and N-terminal domains of the yeast subunits will fill this region, thus allowing the molecule to have a reliable communication system between its distant catalytic sites, which is essential for the functioning of an allosteric enzyme.

The asymmetry previously observed between the top and the bottom tetramers (Ruiz et al., 2001) also is preserved in the present structure. However, within each tetramer the dimers have the same structure. Our observation indicates that each tetramer is found in a different conformation. Within the framework of an allosteric model for the enzyme kinetics it is possible to analyze in detail the different building blocks of the yeast enzyme. As the dimers are mainly composed of a single bacterial tetramer and the α and β subunits of the yeast enzyme show high similarity it is logical to say that the dimer will show strong cooperativity for the sugar substrate, a hypothesis that is corroborated by the high symmetry observed between the L and the U domains (Fig. 5A). The high similarity of the dimers that form either the top or the bottom tetramer indicate that also this unit of the yeast structure presents a positive cooperativity. However, the asymmetry between the two tetramers in the presence of Fru 6-P seems to point out that when the substrate binds to one tetramer its conformational changes are transmitted to the other tetramer through the terminal regions of the subunits. This second tetramer adapts to the changes and may lose its ability to bind the substrate or at least show a much lower affinity for Fru 6-P. Similar mechanisms in which two halves of a molecule are in different conformations are not unusual (Llorca et al., 1999; Roseman et al., 1996). Currently it is still not known if at saturating substrate concentrations all the subunits have substrates bound. There is an open debate about the binding stoichiometry for both substrates; one group proposed 8 binding sites for Fru 6-P and 16 for ATP (Nissler et al., 1977a,b), while the other group claimed half as many (Laurent et al., 1978, 1979). Our studies of Pfk-1 in the presence of Fru 6-P indicate that one-half of the molecule is in one conformation and the other half in another. As in their native state both tetramers are assumed structurally indistinguishable, we could suggest that the enzyme has the largest number possible binding sites (8 for Fru 6-P and 16 for ATP), but that at any given time only half of them are occupied. A better understanding will be reached when we can fit the X-ray model of the yeast tetramer into each half of the molecule. The fitting of the *E. coli* tetramer into the yeast enzyme has allowed us to localize all the putative Fru

6-P binding sites. Each bacterial tetramer has four active sites; therefore, there are four possible Fru 6-P binding sites per yeast dimer (either catalytic or regulatory). Two of them are located in the external surface of the molecule and the other two in the inner part close to the connections between tetramers. Each subunit that forms the dimer has arisen from an initial gene duplication and fusion event. During this process a mutation rendered one-half of the subunit catalytically inactive, which, still able to bind sugar compounds, acquired a regulatory role (Fothergill-Gilmore and Michels, 1993). An analysis of the sequence has determined that an important aspartate residue (Asp126 in *B. stearothermophilus* numbering), which participates in the catalytic mechanism in the prokaryotic enzymes, is present in the N-terminal domain region but is mutated to a serine in the C-terminal domain. Therefore, two of our putative sites are located in the N-terminal regions of the yeast subunits and contribute to the active site, whereas the other two are the regulatory sites and are located in the C-terminal regions of the subunits. It is, therefore, logical to assume that in our structure the two external sites are the active sites and the two inner ones close to the tetramer connections are the sugar effector binding sites.

The results reported here represent a major step in the understanding of the structure of eukaryotic phosphofructokinases. Beyond the immediate results shown here, this three-dimensional reconstruction, obtained by cryoelectron microscopy, has been used in combination with molecular replacement of the *E. coli* tetramer to calculate the initial phases to solve the X-ray structure (manuscript in preparation). To our knowledge similar situations in which electron microscopy has contributed to phasing X-ray data, when no crystallographic heavy-atom derivative data were available, have been restricted to highly symmetric virus structures (Prasad et al., 1999; Simpson et al., 2001; Wang et al., 1997; Wikoff et al., 2000). In the case of the ribosome the molecular envelope was used to localize the bound heavy atoms in the derivatives using difference Fourier maps (Ban et al., 1998).

Acknowledgments

We thank Jürgen Kirchberger and Anke Edelmann, for interesting discussions, and Montserrat Barcena and Radostina Petrova for their continuous interest in the project and their constructive critique of the manuscript.

References

- Ban, N., Freeborn, B., Nissen, P., Penczek, P., Grassucci, R.A., Sweet, R., Frank, J., Moore, P.B., Steitz, T.A., 1998. A 9 Å resolution

- X-ray crystallographic map of the large ribosomal subunit. *Cell* 93, 1105–1115.
- Bär, J., Schellenberger, W., Kopperschläger, G., 1997. Purification and characterization of phosphofructokinase from the yeast *Kluyveromyces lactis*. *Yeast* 13, 1309–1317.
- Blangy, D., 1968. Phosphofructokinase from *E. coli*: evidence for a tetrameric structure of the enzyme. *FEBS Lett.* 2, 109–111.
- Evans, P.R., 1992. Activity and allosteric regulation in bacterial phosphofructokinase. In: Proceedings of the Robert A. Welch Foundation Conference on Chemical Research. XXXVI. Regulation of Proteins by Ligands, (The Robert A. Welch Foundation, Houston), pp. 39–54.
- Evans, P.R., Farrants, G.W., Lawrence, M.C., 1986. Crystallographic structure of allosterically inhibited phosphofructokinase at 7 Å resolution. *J. Mol. Biol.* 191, 713–720.
- Evans, P.R., Hudson, P.J., 1979. Structure and control of phosphofructokinase from *Bacillus stearothermophilus*. *Nature* 279, 500–504.
- Fernandez, J.-J., Sanjurjo, J.R., Carazo, J.-M., 1997. A spectral estimation approach to contrast transfer function detection in electron microscopy. *Ultramicroscopy* 68, 267–295.
- Fothergill-Gilmore, L.A., Michels, P.A., 1993. Evolution of glycolysis. *Prog. Biophys. Mol. Biol.* 59, 105–235.
- Frank, J., Agrawal, R.K., 1998. The movement of tRNA through the ribosome. *Biophys. J.* 74, 589–594.
- Heinisch, J., 1986. Isolation and characterization of the two structural genes coding for phosphofructokinase in yeast. *Mol. Gen. Genet.* 202, 75–82.
- Heinisch, J., Ritzel, R.G., von Borstel, R.C., Aguilera, A., Rodicio, R., Zimmermann, F.K., 1989. The phosphofructokinase genes of yeast evolved from two duplication events. *Gene* 78, 309–321.
- Heinrich, R., Rapoport, S.M., Rapoport, T.A., 1977. Metabolic regulation and mathematical models. *Prog. Biophys. Mol. Biol.* 32, 1–82.
- Hofmann, E., 1976. The significance of phosphofructokinase to the regulation of carbohydrate metabolism. *Rev. Physiol. Biochem. Pharmacol.* 75, 1–68.
- Hofmann, E., Kopperschläger, G., 1982. Phosphofructokinase from yeast. *Methods Enzymol.* 90, 49–60.
- Jones, T.A., Bergoll, M., Kjeldgaard, M., 1990. O: a macromolecular modeling environment. In: Ealick, C.B.A.S. (Ed.), *Crystallographic and Modeling Methods in Molecular Design*. Springer-Verlag, Berlin, pp. 189–195.
- Kopperschläger, G., Bär, J., Nissler, K., Hofmann, E., 1977. Physicochemical parameters and subunit composition of yeast phosphofructokinase. *Eur. J. Biochem.* 81, 317–325.
- Kotlarz, D., Buc, H., 1982. Phosphofructokinases from *Escherichia coli*. *Methods Enzymol.* 90, 60–70.
- Larsson, C., Pahlman, I.L., Gustafsson, L., 2000. The importance of ATP as a regulator of glycolytic flux in *Saccharomyces cerevisiae*. *Yeast* 16, 797–809.
- Laurent, M., Chaffotte, A.F., Tenu, J.P., Roucoux, C., Seydoux, F.J., 1978. Binding of nucleotides AMP and ATP to yeast phosphofructokinase: evidence for distinct catalytic and regulatory subunits. *Biochem. Biophys. Res. Commun.* 80, 646–652.
- Laurent, M., Seydoux, F.J., Dessen, P., 1979. Allosteric regulation of yeast phosphofructokinase. Correlation between equilibrium binding, spectroscopic and kinetic data. *J. Biol. Chem.* 254, 7515–7520.
- Llorca, O., Smyth, M.G., Carrascosa, J.L., Willison, K.R., Radermacher, M., Steinbacher, S., Valpuesta, J.M., 1999. 3D reconstruction of the ATP-bound form of CCT reveals the asymmetric folding conformation of a type II chaperonin. *Nat. Struct. Biol.* 6, 639–642.
- Lorberg, A., Kirchrath, L., Ernst, J.F., Heinisch, J.J., 1999. Genetic and biochemical characterization of phosphofructokinase from the opportunistic pathogenic yeast *Candida albicans*. *Eur. J. Biochem.* 260, 217–226.
- Mouche, F., Boisset, N., Lamy, J., Zal, F., Lamy, J.N., 1999. Structural comparison of cephalopod hemocyanins: phylogenetic significance. *J. Struct. Biol.* 127, 199–212.
- Nissler, K., Hofmann, E., Stel'maschchuk, V., Orlova, E., Kiselev, N., 1985. An electron microscopy study of the quaternary structure of yeast phosphofructokinase. *Biomed. Biochim. Acta* 44, 251–259.
- Nissler, K., Kessler, R., Schellenberger, W., Hofmann, E., 1977a. Binding of fructose-6-phosphate to phosphofructokinase from yeast. *Biochem. Biophys. Res. Commun.* 79, 973–978.
- Nissler, K., Otto, A., Schellenberger, W., Hofmann, E., 1983. Similarity of activation of yeast phosphofructokinase by AMP and fructose-2,6-bisphosphate. *Biochem. Biophys. Res. Commun.* 111, 294–300.
- Nissler, K., Otto, A., Schellenberger, W., Hofmann, E., 1984. Cooperation of fructose-2,6-bisphosphate and AMP in the activation of yeast phosphofructokinase. *Biomed. Biochim. Acta* 43, 535–540.
- Nissler, K., Schellenberger, W., Hofmann, E., 1977b. Binding of MgATP to yeast phosphofructokinase. *Acta Biol. Med. Ger.* 36, 1027–1033.
- Plietz, P., Damaschun, G., Kopperschläger, G., Müller, J.J., 1978. Small-angle X-ray scattering studies on the quaternary structure of phosphofructokinase from baker's yeast. *FEBS Lett.* 91, 230–232.
- Poorman, R.A., Randolph, A., Kemp, R.G., Heinrikson, R.L., 1984. Evolution of phosphofructokinase—gene duplication and creation of new effector sites. *Nature* 309, 467–469.
- Prasad, B.V., Hardy, M.E., Dokland, T., Bella, J., Rossmann, M.G., Estes, M.K., 1999. X-ray crystallographic structure of the Norwalk virus capsid. *Science* 286, 287–290.
- Radermacher, M., 1997. Radon transform techniques for alignment and 3D reconstruction from random projections. *Scanning Microsc. Int. Suppl.*, in press.
- Radermacher, M., 2001. Appendix: simultaneous rotational and translational alignment. *J. Struct. Biol.* 135, 35–37.
- Radermacher, M., Ruiz, T., Wiczorek, H., Grüber, G., 2001. The structure of the VI-ATPase determined by three-dimensional electron microscopy of single particles. *J. Struct. Biol.* 135, 26–37.
- Reuter, R., Eschrich, K., Schellenberger, W., Hofmann, E., 1979. Kinetic modelling of yeast phosphofructokinase. *Acta Biol. Med. Ger.* 38, 1067–1079.
- Reuter, R., Naumann, M., Bär, J., Haferburg, D., Kopperschläger, G., 2000. Purification, molecular and kinetic characterization of phosphofructokinase-1 from the yeast *Schizosaccharomyces pombe*: evidence for an unusual subunit composition. *Yeast* 16, 1273–1285.
- Roseman, A.M., Chen, S., White, H., Braig, K., Saibil, H.R., 1996. The chaperonin ATPase cycle: mechanism of allosteric switching and movements of substrate-binding domains in GroEL. *Cell* 87, 241–251.
- Ruiz, T., Kopperschläger, G., Radermacher, M., 2001. The first three-dimensional structure of phosphofructokinase from *Saccharomyces cerevisiae* determined by electron microscopy of single particles. *J. Struct. Biol.* 136, 167–180.
- Rypniewski, W.R., Evans, P.R., 1989. Crystal structure of unliganded phosphofructokinase from *Escherichia coli*. *J. Mol. Biol.* 207, 805–821.
- Saxton, W.O., Baumeister, W., 1982. The correlation averaging of a regularly arranged bacterial cell envelope protein. *J. Microsc.* 127, 127–138.
- Shirakihara, Y., Evans, P.R., 1988. Crystal structure of the complex of phosphofructokinase from *Escherichia coli* with its reaction products. *J. Mol. Biol.* 204, 973–994.
- Simpson, A.A., Leiman, P.G., Tao, Y., He, Y., Badasso, M.O., Jardine, P.J., Anderson, D.L., Rossmann, M.G., 2001. Structure determination of the head–tail connector of bacteriophage phi29. *Acta Crystallogr. D Biol. Crystallogr.* 57, 1260–1269.
- Sols, A., 1981. Multimodulation of enzyme activity. *Curr. Top. Cell. Regul.* 19, 77–101.

- Stewart, P.L., Chiu, C.Y., Haley, D.A., Kong, L.B., Schlessman, J.L., 1999. Resolution issues in single-particle reconstruction. *J. Struct. Biol.* 128, 58–64.
- Tijane, M.N., Seydoux, F.J., Hill, M., Roucoux, C., Laurent, M., 1979. Octameric structure of yeast phosphofructokinase as determined by crosslinking with disuccinimidyl beta-hydroxybenzoate. *FEBS Lett.* 105, 249–253.
- Uyeda, K., 1979. Phosphofructokinase. *Adv. Enzymol.* 48, 193–244.
- van Heel, M., Keegstra, W., Schutter, W., van Bruggen, E.J.F., 1982. Arthropod hemocyanin structures studied by image analysis. In: Woods, E.J. (Ed.), *Life Chemistry Reports, Suppl.1, The Structure and Function of Invertebrate Respiratory Proteins*. EMBO Workshop, pp. 69–73.
- van Schaftingen, E., 1987. Fructose 2,6-bisphosphate. *Adv. Enzymol. Relat. Areas Mol. Biol.* 59, 315–395.
- Wang, J., Hartling, J.A., Flanagan, J.M., 1997. The structure of ClpP at 2.3 Å resolution suggests a model for ATP-dependent proteolysis. *Cell* 91, 447–456.
- Wikoff, W.R., Liljas, L., Duda, R.L., Tsuruta, H., Hendrix, R.W., Johnson, J.E., 2000. Topologically linked protein rings in the bacteriophage HK97 capsid. *Science* 289, 2129–2133.